Resonance Raman Examination of the Electronic Excited States of Glycylglycine and Other Dipeptides: Observation of a Carboxylate→Amide Charge Transfer Transition

X. G. Chen,[†,‡] Pusheng Li,[‡] Janet S. W. Holtz,[‡] Zhenhuan Chi,[‡] Vasil Pajcini,[‡] Sanford A. Asher,*[,‡] and Lisa A. Kelly[§]

Contribution from the Department of Chemistry, University of Pittsburgh, Pittsburgh, Pennsylvania 15260, and Biology Department, Brookhaven National Laboratory, Upton, New York 11973

Received February 8, 1996[⊗]

Abstract: We have examined the UV resonance Raman and the VUV absorption spectra of aqueous glycylglycine and other dipeptides. We observe strong resonance Raman enhancement of the amide I, II, and III bands and the amide $C_\alpha H$ bending mode in a manner similar to that we observed previously with excitation within the $\pi\rightarrow\pi^*$ transition of N-methylacetamide (Chen, X. G.; Asher, S. A.; Schweitzer-Stenner, R.; Mirkin, N. G.; Krimm, S. *J. Am. Chem. Soc.* **1995**, *117*, 2884). However, in addition, we observe strong resonance Raman enhancement of the ca. 1400 cm^{-1} symmetric COO^- stretching vibration, whose 206.5 nm Raman cross section is increased 20-fold compared to that of the carboxylate in sodium acetate, for example. Addition of a methylene spacer between the amide and carboxylate groups causes the resonance Raman enhancement of this symmetric COO^- stretch to disappear. The UV resonance Raman excitation profiles, the Raman depolarization ratio dispersion, and the VUV absorption spectra of glycylglycine and other dipeptides demonstrate the existence of a new 197 nm charge transfer band which involves electron transfer from a nonbonding carboxylate orbital to the amide-like π^* orbital. This transition occurs at the penultimate carboxylate end of all peptides and proteins.

Introduction

Glycylglycine (Gly-Gly) and other dipeptides have served as important model systems for theoretical[1−6] and experimental studies[7−13] of the amide linkage in proteins and peptides. The study of these species has been motivated by the expectation that a fundamental understanding of protein structural constraints, and their role in controlling biological function, requires a deep understanding of the structure and dynamics of the individual peptide amide linkages.

The ground state structure of Gly-Gly and other dipeptides has been characterized by a wide variety of techniques.[14−18] The early X-ray diffraction[14] and neutron diffraction[15] data suggested that the amide and carboxylate planes are not parallel, and that a small torsional angle exists between the amide and carboxylate planes in Gly-Gly crystals. This angle shows significant variations between different crystal structures.[16,17] NMR dipeptide studies[18] indicate that a large number of conformers with various torsional angles exist in aqueous solution. The preferred conformation, however, is an eclipsed structure between the COO^- and NH_3^+ ion pairs, which minimize the distance between them.[18] The key conformational determinants for dipeptides in water are believed to be the terminal ion pair interactions and the solvation of the amide group and of the side chains.[18] Recent ground state geometry *ab initio* calculations[1] suggest that "blocked" dialanine ($CH_3CH_2CONHCH_2CONHCH_2CH_3$) and "blocked" diglycine ($CH_3CONHCH_2CONHCH_3$) favor helical conformations in aqueous solution.

Little information exists on the electronic excited state structure of Gly-Gly and other dipeptides.[6−11] Recent UV resonance Raman (UVRR) measurements[9b,10a] of trans *N*-methylacetamide (NMA) in water have demonstrated facile monophotonic photoisomerization to the cis isomer of the ground state upon excitation within the amide $\pi\rightarrow\pi^*$ transition; this result could indicate a nonplanar excited state geometry. Indeed, recent *ab initio* theoretical excited state calculations find twisted excited states for isolated NMA.[6] More recently, UVRR

* Author to whom correspondence should be addressed.
† Present Address: Section on Metabolic Analysis and Mass Spectrometry, NICHD, National Institutes of Health, 10 Center Drive, MSC 1580, Building 10, Room 6C208, Bethesda, MD 20892.
‡ University of Pittsburgh.
§ Brookhaven National Laboratory.
⊗ Abstract published in *Advance ACS Abstracts,* October 1, 1996.

(1) (a) Shang, H. S.; Head-Gordon, T. *J. Am. Chem. Soc.* **1994**, *116*, 1528. (b) Head-Gordon, T.; Head-Gordon, M.; Frisch, M. J.; Brooks, C. L., III; Pople, J. A. *J. Am. Chem. Soc.* **1991**, *113*, 5989.
(2) Ryan, J. A.; Whitten, J. L. *J. Am. Chem. Soc.* **1972**, *94*, 2396.
(3) Petke, J. D. *J. Chem. Phys.* **1990**, *93*, 2561.
(4) Pellegrini, M.; Doniach, S. *J. Chem. Phys.* **1995,** *103*, 2696.
(5) Stites W. E.; Pranata, J. *Protein Struct. Funct. Gen.* **1995** 22, 132.
(6) Li, Y.; Garrell, R. L.; Houk, K. N. *J. Am. Chem. Soc.* **1991**, *113*, 5895.
(7) Robin, M. B. *Higher Excited States of Polyatomic Molecules*; Academic Press: Orlando, 1975; Vol. II.
(8) Hill, R. R.; Coyle, J. D.; Birch, D.; Dawe, E.; Jeffs, G. E.; Randall, D.; Stec, I.; Stevenson, T. M. *J. Am. Chem. Soc.* **1991**, *113*, 1805.
(9) (a) Krimm, S.; Song, S.; Asher, S. A. *J. Am. Chem. Soc.* **1989**, *111*, 4290. (b) Song, S.; Asher, A. S.; Krimm, S.; Shaw, K. D. *J. Am. Chem. Soc.* **1991**, *113*, 1155. (c) Song, S.; Asher, S. A. *J. Am. Chem. Soc.* **1989**, *111*, 4295.
(10) (a) Wang, Y.; Purrello, R.; Georgiou, S.; Spiro, T. G. *J. Am. Chem. Soc.* **1991**, *113*, 6359. (b) Wang, Y.; Purrello, R.; Spiro, T. G. *J. Am. Chem. Soc.* **1989**, *111*, 8274.
(11) Clark, L. B. J. *Am. Chem. Soc.* **1995**, *117*, 7974.
(12) Klapstein, D.; Olivato, P. R.; Oike, F.; Martins, M. A. P.; Rittner, R. *Can. J. Spectrosc.* **1988**, *33*, 161.
(13) Miyazawa, M.; Kyogoku, Y.; Sugeta, H. *Spectrochim. Acta* **1994**, *50A*, 1505.
(14) (a) Biswas, A. B.; Hughes, E. W.; Sharma, B. D.; Wilson, J. N. *Acta Crystallogr.* **1968**, *B24*, 40. (b) Hughes, E. W *Acta Crystallogr.* **1968**, *B24*, 1128.
(15) Freeman, H. C.; Paul, G. L. *Acta Crystallogr.* **1970**, *B26*, 925.
(16) Pajcini, V.; Chen, X. G.; Bormett, R. W.; Geib, S. J.; Li, P.; Asher, S. A.; Lidiak, E. G. *J. Am. Chem. Soc.* **1996**, *118*, 9716 (following paper in this issue).
(17) Koetzle, T. F.; Hamilton, W. C. *Acta Crystallogr.* **1972**, *B28*, 2083.
(18) Beeson, C.; Dix, T. A. *J. Chem. Soc., Perkin. Trans. 2* **1991**, 1913.

S0002-7863(96)00421-0 CCC: $12.00

studies revealed that the $\pi\pi^*$ excited state geometry[19,20] of NMA in water differs from that of ground state, in that the amide CN and CO bonds elongate, while the CH_3-C and the $N-CH_3$ bonds contract.

The energy and geometry of the amide $\pi\pi^*$ excited state in dipeptides is likely to differ from that of NMA, because electronic interactions may occur between the adjacent carboxylate and amide chromophores. These interactions may shift the amide $\pi\rightarrow\pi^*$ electronic transition or create new electronic transitions.[21,22] For blocked diglycine, the strongest absorption band in the vacuum UV has been calculated[3] to derive from an electronic transition to an "exciton-like" state arising from the electronic coupling between the two local amide π^* orbitals. A $\pi\rightarrow\pi^*$ charge transfer transition from one amide group to another is predicted to occur at even higher energy. Similar couplings between the amide and carboxylate groups should be expected in dipeptides. The magnitude of this electronic coupling will depend on the energy differences between the chomophore orbitals, the orientation between the coupled electronic transitions, as well as on the solvent environment[21,22]

The understanding of electronic excited state coupling between peptide amide groups in proteins may reveal any possible role of peptide bonds as conduits through which photoinduced[23] or ground state electron transfer[24] occurs in proteins. Previous photochemical studies[8] of aqueous dipeptides suggested that a photoinduced electron-transfer process from the carboxylate group to the peptide bond occurs upon UV irradiation. In the gas phase, Weinkauk *et al*. observed[25] charge migration through the peptide backbone in small peptides upon local photoionization of the aromatic side groups. The charge transfer process was suggested to result from photon excitation directly into a delocalized charge transfer transition band, or into a localized excited state, followed by nonradiative relaxation to the charge transfer state. However, no such charge transition bands were observed in the numerous previous absorption spectral studies[26−28] of dipeptides.

In this work, we have utilized UV RR and VUV absorption spectra to examine the electronic transitions and excited states of glycylglycine and other dipeptides in water. We demonstrate that the resonance Raman excitation profiles and Raman depolarization ratios are very sensitive to the presence of electronic coupling between the carboxylate and amide groups, and to the orientation between the coupled electronic transitions. Our results indicate that a charge transfer band at ca. 197 nm occurs in aqueous glycylglycine and other dipeptides, which results from electronic interactions between the amide and carboxylate groups. The charge transfer band involves electron transfer from a carboxylate nonbonding orbital to the amide π^* orbital.

Experimental Section

Materials. *N*-Methylacetamide ($CH_3CONHCH_3$, NMA) was purchased from Aldrich Chemical Co. and distilled before use. Glycyl-β-alanine ($H_2NCH_2CONHCH_2CH_2COOH$, Gly-β-Ala) and the various amino acid monomers (other than glycine) were purchased from Sigma Chemical Co. *N*-Acetylglycine ($CH_3CONHCH_2COOH$, Ace-Gly), glycylglycine ($H_2NCH_2CONHCH_2COOH$, Gly-Gly), glycine (Gly), glycine methyl ester hydrochloride, and D_2O were obtained from Aldrich Chemical Co. Sodium acetate, formic acid (FC), glutaric acid, and butyric acid, all of the highest purity available, were obtained from Aldrich Chemical Co. *N*-Acetyl-β-alanine ($CH_3CONHCH_2CH_2COOH$, Ace-β-Ala) was obtained from Pfaltz & Bauer. All compounds were used without further purification, unless specified.

Glycylglycine-$^{13}C_1$ ($H_2NCH_2CONHCH_2{}^{13}COOH$, Gly-Gly-$^{13}C_1$) was prepared by catalytic hydrogenation of its protected derivative, carbobenzyloxyglycineglycine-$^{13}C_1$, in 1:1 methanol−water at atmospheric pressure. The carbobenzyloxyglycylglycine-$^{13}C_1$ was synthesized from carbobenzyloxyglycine-*p*-nitrophenyl ester (Aldrich Chemical Co.) according to the procedure of Swenson and Koob.[29]

N-Carbobenzyloxy-2-methylalanylglycine methyl ester was synthesized from the reaction of *N*-carbobenzyloxy-2-methylalanine (Aldrich Chemical Co.) with glycine methyl ester. The product was separated from the reaction mixture on a silica column, and then hydrolyzed by 1 M LiOH to give *N*-carbobenzyloxy-2-methylalanyl-glycine. 2-Methylalanylglycine was obtained from *N*-carbobenzyloxy-2-methylalanylglycine by catalytic hydrogenation over Pd/C in methanol solution at a pressure of 50 psi, followed by recrystalization in a mixture of water and methanol.

N-Acetylglycine-$^{13}C_1$ ($CH_3CONHCH_2{}^{13}COOH$, Ace-Gly-$^{13}C_1$) was prepared by adding acetyl chloride to glycine-$^{13}C_1$ in tetrahydrofuran containing 2 equiv of NaOH at 0 °C. Likewise *N*-acetylglycine-$^{13}C_2$ ($CH_3CONH{}^{13}CH_2COOH$, Ace-Gly-$^{13}C_2$) and *N*-trimethylacetylglycine ($(CH_3)_3CCONHCH_2COOH$, TMA-Gly) were prepared by the reaction of acetyl chloride with glycine-$^{13}C_2$ and trimethylacetyl chloride with glycine, respectively. The identities and purities of the final products were confirmed by proton NMR and mass spectral measurements.

L-Alanyl-*d*-L-alanine was a gift from Professor Max Diem from Hunter College of the City University of New York.

Instrumentation. UV resonance Raman (UVRR) spectra were obtained by using a ca. 135° back-scattering geometry, and by exciting samples flowing through a 1.0 mm i.d. suprasil quartz capillary, in a spinning quartz cell, or by utilizing a microsampling flow system.[30] The UVRR spectrometer is described in detail elsewhere.[31] A variety of laser excitation sources were utilized. We utilized a Quanta-Ray DCR-2A Nd:YAG pulsed laser, in which the 1.06 μm fundamental was frequency doubled to pump a dye laser at a 20-Hz repetition rate. The dye laser output was frequency doubled and mixed with the YAG fundamental to generate excitation wavelengths throughout the 220−300-nm region. Other laser excitation sources utilized intra-cavity frequency doubled CW Ar^+ and Kr^+ laser sources[31,32] to generate excitation frequencies at 244 and 228.9 nm, and at 206.5 nm, respectively. The 210-nm excitation was obtained by doubling the output of a 100 Hz repetition rate XeCl excimer laser-pumped dye laser.[33]

The Raman scattered light was dispersed by a Spex Triplemate monochromator and detected by either an EG&G PAR 1420 blue-intensified Reticon diode array or by an intensified CCD detector (Princeton Instrument Co.). Raman cross sections were obtained by comparing the analyte band intensities to the Raman intensity of internal

(19) (a) Chen, X. G.; Asher, S. A.; Schweitzer-Stenner, R.; Mirkin, N. G.; Krimm, S. *J. Am. Chem. Soc.* **1995**, *117*, 2884. (b) Chen, X. G.; Schweitzer-Stenner, R.; Asher, S. A.; Mirkin, N. G.; Krimm, S. *J. Phys. Chem.* **1995**, *99*, 3074.

(20) (a) Hudson, B. S. In press. (b) Mayne, L. C.; Hudson, B. *J. Phys. Chem.* **1991**, *95*, 2962.

(21) Schellman, J. A.; Becktel, W. J. *Biopolymers* **1983**, *22*, 171.

(22) Tinoco, I., Jr.; Cantor, C. R. *Methods Biochem. Anal.* **1970**, 18, 81.

(23) Wasielewski, M. R. In *Photoinduced Electron Transfer;* Fox, M. A., Chanon, M., Eds.; Elsevier: Amsterdam, 1988; Part A, p 161.

(24) Isied, S. S. *Electron Transfer Inorg. Org. Biol. Syst.* **1991**, *228*, 229.

(25) Weinkauf, R.; Schanen, P.; Yang, D.; Soukara, S.; Schlag, E. W. *J. Phys. Chem.* **1995**, *99*, 11255.

(26) (a) Neilsen, E. B.; Schellman, J. A. *J. Phys. Chem.* **1967**, *71*, 2297. (b) Schellman, J. A.; Neilsen, E. B. *J. Phys. Chem.* **1967**, *71*, 3914.

(27) (a) Kaya, K.; Nagakuru, S. *J. Mol. Spectrosc.* **1972**, *44*, 279. (b) Kaya, K.; Nagakuru *Theor. Chim. Acta* **1967**, 117.

(28) Saidel, L. J. *Arch. Biochem. Biophys.* **1955**, *56*, 45.

(29) Swenson, C. A.; Koob, L. J. *J. Phys. Chem.* **1970**, *74*, 3376.

(30) Chen, X. G.; Lemmon, D. H.; Bormett, R. W.; Asher, S. A. *Appl. Spectrosc.* **1993**, *47*, 248.

(31) (a) Asher, S. A. *Anal. Chem.* **1993**, *65*, 59A. (b) Asher, S. A. *Anal. Chem.* **1993**, *65*, 201A. (c) Asher, S. A.; Bormett, R. W.; Chen, X. G.; Lemmon, D. H.; Cho, N.; Peterson, P.; Arrigoni, M.; Spinelli, L.; Cannon, J. *Appl. Spectrosc.* **1993**, *47*, 628.

(32) Holtz, J. S. W; Bormett, R. W.; Chi, Z.; Cho, N.; Chen, X. G.; Pajcini, V.; Asher, S. A.; Spinelli, L.; Owen, P.; Arrigoni, M. *Appl. Spectrosc.* In press.

(33) Jones, C. M.; Devito, V. L.; Harmon, P. A.; Asher, S. A. *Appl. Spectrosc.* **1987**, *41*, 1268.

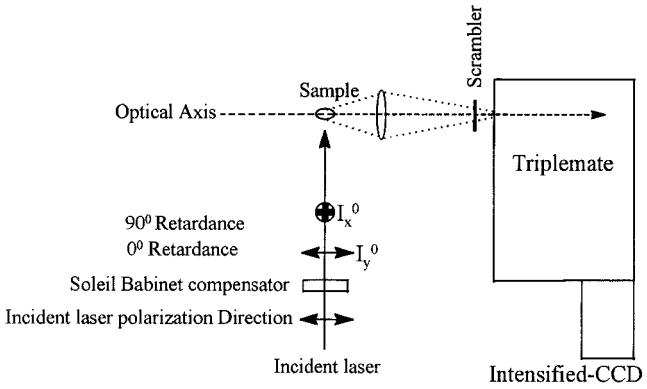

Figure 1. Block diagram of the experimental layout for the depolarization ratio measurements for $\lambda_{ex} < 244$ nm.

standards, such as ClO_4^-, which have known Raman cross sections.[34] These data were corrected for variations in spectrometer efficiency and in detector pixel sensitivity, and for self absorption, if necessary. The maximum irradiation time was 25 min.

For excitation wavelengths greater than 244 nm depolarization ratios, ρ, were measured with either a 180° or 135° scattering geometry by utilizing a calibrated Polacoat polarization analyzer placed in front of the polarization scrambler before the monochromator entrance slit. The UV transmittance of the Polacoat polarization analyzer was too low for use with excitation wavelengths below 244 nm. For $\lambda_{ex} < 244$ nm, ρ was measured by using a 90° scattering geometry by rotating the polarization of the incident beam as shown in Figure 1. The incident beam polarization was aligned to be either parallel or perpendicular to the light collection optical axis, by using a quartz Soleil−Babinet compensator placed before the sample to generate the desired orthogonal polarizations. The incident laser power fluctuated by less than 1%.

For $\lambda_{ex} > 244$ nm, ρ was calculated as the ratio of Raman intensities measured with the polarization analyzer oriented perpendicular, $I_\perp$, and parallel, $I_{||}$, to the incident polarization:

$$\rho = I_\perp / I_{||} \tag{1}$$

When the excitation beam polarization was rotated ($\lambda_{ex} < 244$ nm), ρ was calculated from[35a]

$$\rho = I_x/(2I_y - I_x) \tag{2}$$

where I_x and I_y are Raman intensities collected with the incident beam polarized either perpendicular, I_x^0, or parallel, I_y^0, to the light collection axis, respectively (Figure 1).

The accuracy of the depolarization ratio measurements was checked by measuring the depolarization ratio of the Raman bands of CCl_4, ClO_4^-, CH_3CN, and cyclohexane, which served as the depolarization ratio standards.[35] For the nonabsorbing sample solutions, we observed negligible errors in our depolarization ratio measurements. In contrast, absorbing sample solutions showed significant depolarization ratio measurement errors ($\lambda_{ex} < 244$ nm). We, therefore, corrected our measured depolarization ratios, ρ_{obs}, with the use of the following expression,[35a]

$$\rho = \frac{\rho_{obs}(2 - \delta_x) - \delta_x}{2 - 4\rho_{obs}\delta_y} \tag{3}$$

where δ_x and δ_y are the relative errors, $\Delta I_x/I_y^0$ and $\Delta I_y/I_x^0$, due to incomplete polarization of the light parallel and perpendicular to the spectrometer optical axis (Figure 1). The δ_x and δ_y values were determined by a least-squares fitting of the known ρ values of the different Raman bands of the standards to the observed, ρ_{obs}, values measured in the absorbing medium. The calculated δ_x and δ_y values for 206.5-nm excitation were 0.04 and −0.03, respectively.

(34) Dudik, J. M.; Johnson, C. R.; Asher, S. A. *J. Chem. Phys.* **1985**, *82*, 1732.

(35) (a) DeVito, V. L.; Asher, S. A. *J. Phys. Chem. Soc.* **1992**, *96*, 6917. (b) DeVito, V. L.; Asher, S. A. *J. Am. Chem. Soc.* **1989**, *111*, 9143.

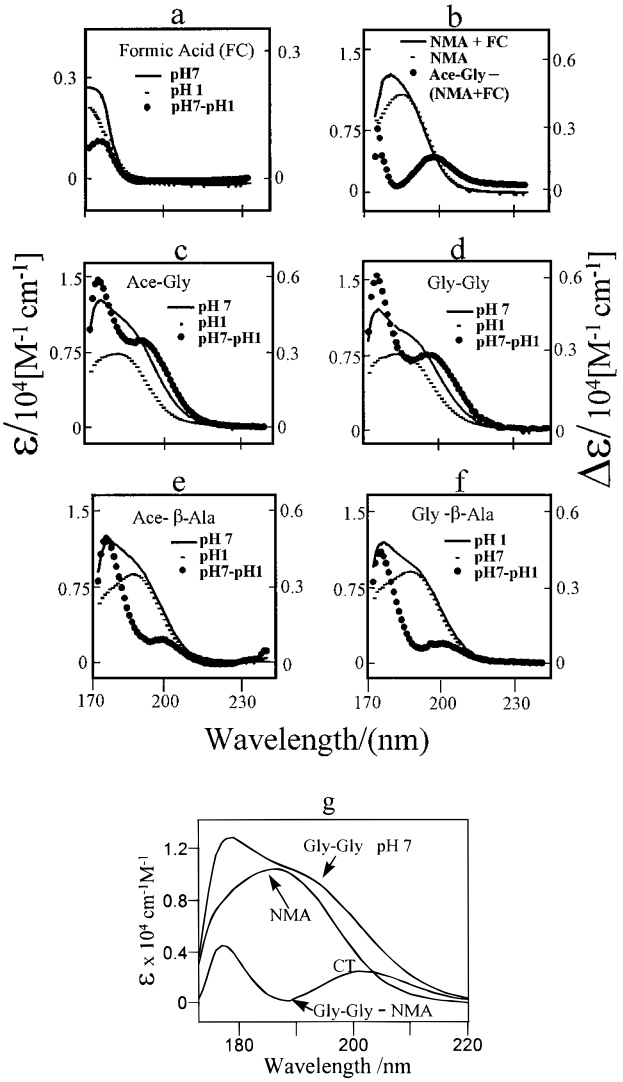

Figure 2. VUV absorption spectra of aqueous formic acid (FC), *N*-methylacetamide (NMA), acetylglycine (Ace-Gly), glycylglycine (Gly-Gly), acetyl-β-alanine (Ace-β-Ala), and glycyl-β-alanine (Gly-β-Ala) at pH 7 and 1, their pH absorption difference spectra, and the absorption difference spectra between Ace-Gly and the sum of absorption spectra of NMA and FC. Part g shows the absorption difference spectrum between Gly-Gly at pH 7 and NMA. All spectra we obtained by measuring the pseudoabsorption spectra and rescaled to absorption spectra measured for $\lambda > 185$ nm (see text for detail). The sample solution concentration was ca. 0.6 M.

Vacuum UV spectra were obtained by measuring the pseudoabsorption spectra at the National Bureau of Standard's Synchrotron Ultraviolet Radiation Facility at Brookhaven National Laboratory.[36] For these measurements ca. 0.6 M sample solutions were prepared, to give absorbances of ca. 1.0 at 190 nm for ca. 12.5 μm optical path length. Because the exact path length was unknown, these spectra were scaled to spectra measured for $\lambda > 185$ nm by using a nitrogen purged Perkin-Elmer Model Lambda 9 UV−VIS−NIR spectrophotometer.

Results

VUV Absorption Spectra. Figure 2 shows the pH dependence of the VUV absorption spectra of aqueous solutions of various simple acids and dipeptides in the region between 170 and 240 nm, while Table 1 lists some of the spectral results. Aqueous formic acid (FC) at pH 7 (Figure 2a) exhibits an absorption band with a maximum at ca. 173 nm ($\epsilon \approx 3000$ M^{-1}

(36) Sutherland, J. C.; Keck, P. C.; Griffin, K. P.; Takacs, P. Z. *Nucl. Instrum. Methods* **1982**, 195,375.

(37) Albrecht, A. C.; Hutley, M. C. J. *J. Chem. Phys.* **1971**, 55, 4438.

Table 1. Assignments of Absorption Bands of Aqueous Formic Acid, *N*-Methylacetamide, Acetylglycine, and Glycylglycine[a]

compd	absorption band max (nm)	type	notation[b]	oscillator strength[c]
formic acid (pH 7)	172	$\pi\pi^*$	NV_1	≈0.08
formic acid (pH 1)	≈160	$\pi\pi^*$	NV_1	≈0.05
N-methylacetamide	185	$\pi\pi^*$	NV_1	0.37
acetylglycine (pH 7)[a]	197	charge transfer		0.1
	185	$\pi\pi^*$	amide NV_1	0.37
	172	$\pi\pi^*$	carboxylate NV_1	0.1
acetylglycine (pH 1)	185	$\pi\pi^*$	amide NV_1	0.33
glycylglycine (pH 7)[a]	197	charge transfer		0.12
	185	$\pi\pi^*$	amide NV_1	0.37
	172	$\pi\pi^*$	carboxylate NV_1	0.1
glycylglycine (pH 1)	185	$\pi\pi^*$	amide NV_1	0.34

[a] The absorption spectra are decomposed into three components: an amide-like $\pi\rightarrow\pi^*$ transition, a carboxylate-like $\pi\rightarrow\pi^*$ transition and a new band at 197 nm (Figure 2g). The absorption of the amide-like $\pi\rightarrow\pi^*$ component is assumed to be identical to that of NMA; the oscillator strength of the charge transfer component is calculated by integrating the difference spectrum in the region 183−240 nm. The carboxylate-like $\pi\rightarrow\pi^*$ oscillator strength is estimated by integrating the peak in the difference spectrum between 170−183 nm. [b] See reference 7. [c] The oscillator strengths are estimated by the formula[42] $f = 4.315 \times 10^{-9} \int \epsilon \, d\nu$. Since no absorption data are available below 170 nm, the absorption feature below 170 nm is estimated based on the assumption that each band is symmetric, and that we can estimate the oscillator strength by doubling the integrated intensity from the band center frequency to the low-frequency edge.

cm^{-1}) assigned to the in-plane $\pi\rightarrow\pi^*$ NV_1 transition of the carboxylate group.[7] The oscillator strength of this band is estimated to be ca. 0.08 (Table 1). Upon carboxylate protonation at pH 1 the FC absorption maximum blue shifts.

The strong $\pi\rightarrow\pi^*$ NV_1 transition of *N*-methylacetamide (NMA) occurs at 185 nm (Figure 2b). We calculate the oscillator strength of the aqueous NMA amide $\pi\rightarrow\pi^*$ transition to be ca. 0.37 (Table 1). In contrast to FC, the absorption spectrum of NMA is essentially independent of solution pH. Figure 2b also shows the sum of the spectra of NMA and FC at pH 7.

The Figure 2c and 2d spectra of Ace-Gly and Gly-Gly at pH 7 suggest an interaction between the amide and carboxylate electronic transitions, since Ace-Gly and Gly-Gly at pH 7 show stronger and broader absorption bands than those which occur in the spectral sum of NMA and FC (Figure 2b). The difference spectrum (Figure 2b) between Ace-Gly and the spectral sum of the NMA and FC displays two absorption maxima at 197 and 178 nm, with molar absorptivities of ca. 2200 and ca. 3000 M^{-1} cm^{-1} and oscillator strengths of ca. 0.09 and ca. 0.04, respectively.

Figures 2c and 2d show that a large absorption decrease occurs upon carboxylate protonation of Ace-Gly and Gly-Gly; the pH difference spectrum shows peaks at ca. 197 nm ($\epsilon \approx$ 3000 M^{-1} cm^{-1}) and at 178 nm ($\epsilon \approx$ 6000 M^{-1} cm^{-1}) with oscillator strength of ca. 0.1 and ca. 0.05, respectively. Ace-β-Ala and Gly-β-Ala, which each have an additional methylene group between the amide and the carboxylate groups, also show large absorption difference features around 180 nm. However, at longer wavelengths we observe five-fold smaller pH absorbance difference features which are red shifted to 205 nm (Figures 2e and 2f). The pH difference absorption features of Ace-Gly and Gly-Gly are similar to the difference spectrum observed between Ace-Gly and the sum of NMA and FC spectra (Figure 2b), and to the difference spectrum between aqueous Gly-Gly at pH 7 and NMA (Figure 2g). The high-frequency band at 177 nm is presumably the carboxylate $\pi\rightarrow\pi^*$ transition.

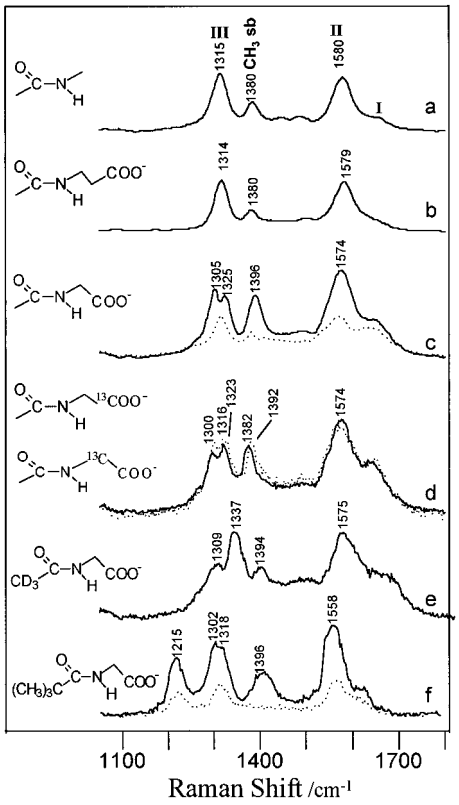

Figure 3. Resonance Raman spectra of (a) *N*-methylacetamide (NMA) in H_2O at pH 7, (b) acetyl-β-alanine (Ace-β-Ala) in H_2O at pH 6, (c) acetylglycine (Ace-Gly) in H_2O at pH 6 (solid line) and pH 1.8 (dotted line), (d) acetylglycine-$^{13}C_1$ (Ace-Gly-$^{13}C_1$) in H_2O at pH 7 (solid line) and acetylglycine-$^{13}C_2$ (Ace-Gly-$^{13}C_2$) in H_2O at pH 6 (dotted line), (e) d_3-acetylglycine (CD_3-Ace-Gly) in H_2O at pH 7, and (f) trimethylacetylglycine (TMA-Gly) in H_2O at pH 6 (solid line) and pH 1.7 (dotted line). Spectra a, b, c, and f are obtained with 206.5-nm excitation, and spectra d and e are obtained with 218-nm excitation. Spectral resolution: ca. 14 cm^{-1} for 206.5 nm, ca. 10 cm^{-1} for 218 nm. The 206.5-nm excitation utilized ca. 3 mW CW laser power, and the spectra were accumulated over a period of ca. 10 min.. The 218 nm excited spectra were obtained at a 20 Hz repetition rate using 6-ns pulses with laser pulse energies of ca. 0.25 mJ with accumulation times of ca. 6 min. The sample concentrations were ca. 5 mM for 206.5-nm excitation and ca. 50 mM for 218-nm excitation.

There appears to be little interaction between the amide and carboxylate electronic transitions in Ace-β-Ala and Gly-β-Ala. The Ace-β-Ala spectrum at pH 7 is similar to the sum of the NMA and FC spectra, while the Ace-β-Ala spectrum at pH 1 is similar to that of NMA, except for an increased absorbance at shorter wavelengths for the protonated carboxyl group (FC at pH 1 in Figure 2a). The strong peak observed at ca. 178 nm in the pH difference spectra is presumably due to the absorption difference between the protonated and deprotonated carboxyl groups.

The 197 nm absorption difference spectral peak appears as a new feature, which results from interactions between the carboxylate and the amide groups across the connecting methylene linkage. The presence of two methylene spacers between the amide and carboxylate groups, such as in Gly-β-Ala and Ace-β-Ala, removes the absorption feature near 197 nm, indicating that this band depends upon the proximity of the amide and carboxylate groups.

The interaction between the non-degenerate amide and carboxylate $\pi\rightarrow\pi^*$ electronic transitions could increase the total number of low-energy electronic transitions. In addition, significant changes in the relative oscillator strengths of the carboxylate and amide $\pi\rightarrow\pi^*$ transitions are expected, if strong

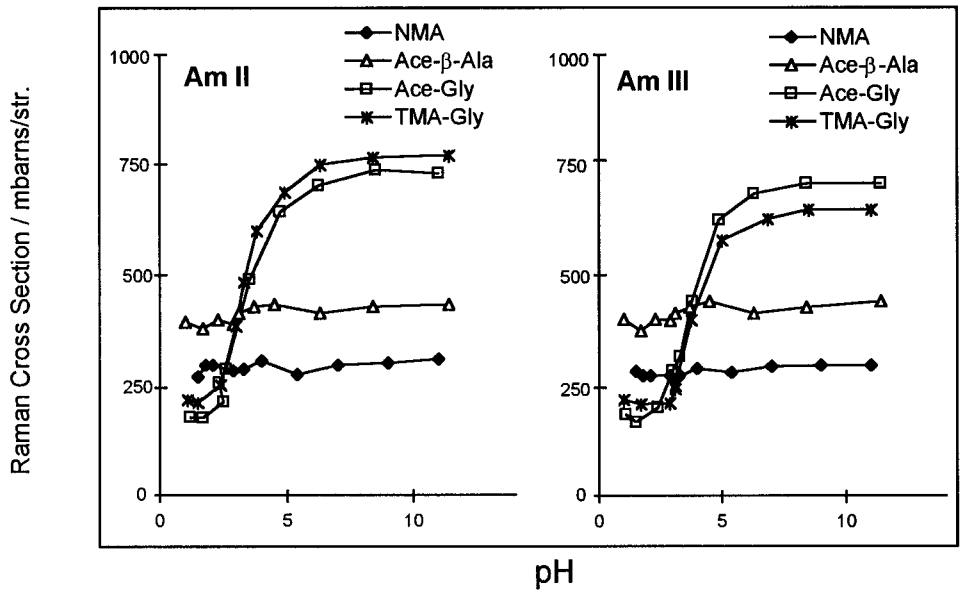

Figure 4. The pH dependence of 206.5 nm excited relative Raman cross sections of the amide II and amide III bands of *N*-methylacetamide (NMA), acetylglycine (Ace-Gly), acetyl-β-alanine (Ace-β-Ala), and trimethylacetylglycine (TMA-Gly).

exciton interactions occur.[22] We have utilized the UV resonance Raman spectral data below to assign these transitions.

UV Resonance Raman Spectra. Figure 3 compares the 206.5-nm excited Raman spectra of NMA, Ace-β-Ala, Ace-Gly isotopomers, and TMA-Gly, while Figure 4 plots the pH dependence of their amide II and III band Raman cross sections. Excitation in resonance with the amide $\pi\rightarrow\pi^*$ transition of aqueous NMA (Figure 3a) enhances the amide I (1635 cm^{-1}), amide II (1580 cm^{-1}), and amide III (1315 cm^{-1}) bands and the $C_\alpha H_3$ methyl symmetric bending band (CH_3 sb 1380 cm^{-1}). These resonance enhancements result from the NMA $\pi\pi^*$ excited state distortion, which elongates the CN bond, contracts the CC and NC bonds, and slightly elongates the CO bond.[19]

The resonance Raman spectrum of Ace-β-Ala (Figure 3b) is nearly identical to that of NMA (Figure 3a), suggesting that the Ace-β-Ala $\pi\pi^*$ excited state geometric distortion is essentially identical to that of NMA, and is not affected significantly by the carboxylate group which is separated from the amide group by two methylene spacers. We assume that the amide vibrational modes of Ace-β-Ala have a similar normal mode composition to those of NMA, which appears reasonable since the frequencies are so similar. The lack of involvement of the carboxylate group electronic transition in the enhancement is also evident from the fact that no pH dependence occurs for the Raman cross sections of the amide bands of Ace-β-Ala (Figure 4). As discussed above, the Ace-β-Ala absorption spectrum (Figure 2e) is relatively pH insensitive.

In contrast, the resonance Raman spectrum of aqueous Ace-Gly at pH 7 (Figure 3c, solid line) differs significantly from that of Ace-β-Ala. The 206.5 nm Raman cross sections of the amide II and III bands of Ace-Gly at pH 7 are increased 2-fold compared to those of Ace-β-Ala, and are increased 4-fold compared to those Ace-Gly at pH 1 (Figure 4). This increase scales roughly with the square of the 206.5 nm molar absorptivity increase. Protonation of Ace-Gly at pH ca. 1 (Figure 3c, dotted line) results in a spectrum reminiscent of NMA, although the relative intensity of the amide I band is somewhat increased.

The spectrum of Ace-Gly at pH 7 shows a strong band at 1396 cm^{-1} which disappears upon carboxylate protonation (Figure 3c, dotted line). The frequency of this band down shifts by 14 cm^{-1} upon $^{13}COO^-$ substitution of Ace-Gly (Figure 3d, solid line). Thus, this 1396-cm^{-1} band is definitively assigned to the COO^- symmetric stretch. C_α deuteration of Ace-Gly to form C-d_3-Ace-Gly (Figure 3e) and methyl substitution to form TMA-Gly (Figure 3f) allow us to clearly observe the symmetric COO^- stretching band, since this deuterium or methyl substitution eliminates the overlapping CH_3 symmetric bending deformation. This 1396-cm^{-1} band disappears at low pH (see TMA-Gly for example, Figure 3f, dotted line) as carboxylate protonation removes the symmetric COO^- stretching vibration. The Raman cross section of the symmetric COO^- stretch of Ace-Gly excited at 206.5 nm is ca. 400 mbarns/str (Table 2), which is 20-fold larger than that for an isolated carboxylate group, such as in Gly or FC (ca. 20 mbarns/str, Table 2).

Table 2. Total Raman Cross Sections

compds	bands (cm^{-1})	σ (mbarn/str) σ_{218}	σ_{206}	$\nu_e{}^a$ (nm)	K^a (10^{-30})
	pH 7				
NMA	1580 (Am II)	4.3	310	188[b]	6.01[b]
	1315 (Am III)	5.8	300	183[b]	4.55[b]
	1380 (CH_3 sb)	1.4	97	186[b]	4.49[b]
Ace-Gly	1638 (Am I)	3.8	270		
	1579 (Am II)	11	790		
	1325/1305(Am III)	13	730		
	1396 (COO^- +CH_3 sb)	10	710		
Acetic acid	1421 (COO^-)	0.43	16	174[c]	11.5[c]
	1354 ($CH_{3\,sb}$)	0.16	4.6	174[c]	2.82[c]
Gly	1411 (COO^-)	0.47	19	172	26.7
	1332 ($CH_{2\,sb}$)	0.18	5.6	172	11.8
Gly pH 1	1744 (CO s)	0.16	5.7		
Gly-Gly	1576 (Am II)	17	1310	195	10.8
	1286 (Am III)	18	1270	195	21.7
	1403 ($C_\alpha H$ sb + COO^-)	17	1280		
	1318 ($C_\beta H$ sb)	2.3	280		
Gly-Gly	1496 (Am II′)	34	2640	194	60.8
(D_2O)	1396 (COO^-)	4.5	280	189	10.8
Gly-β-Ala	1571 (Am II)	13	980		
	1275 (Am III	14	960		
	1396 ($C_\alpha H$ sb)	6.7	510		
TMA-Gly	1558 (Am II)	12	790	196	9.1
	1303/1318 (Am III)	10	730	196	12.4
	1396 (COO^-)	6.0	330	189	4.7
	1216	9.8	530	193	5.1

[a] $\sigma = K\nu_0(\nu_0 - \nu_{mn})^3[(\nu_e^2 + \nu_0^2)/(\nu_e^2 - \nu_0^2)^2]^2$, where ν_0 is the excitation frequency.[19,37] ν_e and K are obtained by non-linear least-squared fits of preresonance Raman data (300 nm < λ < 210 nm) to this equation. [b] See reference 19. [c] See reference 9b.

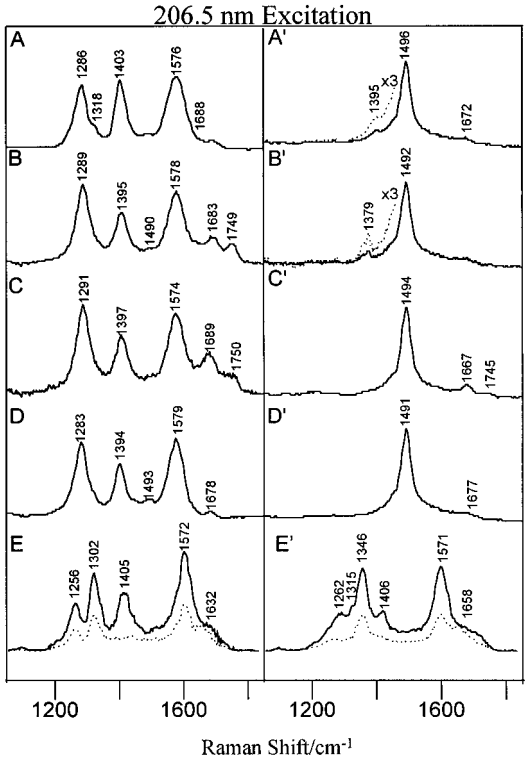

Figure 5. Resonance Raman spectra of (A) glycylglycine (Gly-Gly) in H_2O at pH 6.5, (B) glycylglycine (Gly-Gly) in H_2O at pH 1.7, (C) glycylglycine methyl ester (Gly-Gly-Me) in H_2O at pH 6, (D) glycyl-β-alanine (Gly-β-Ala) in H_2O at pH 6.5, (E) 2-methylalanylglycine in H_2O at pH 6 (solid line) and at pH 1.5 (dotted line), (A′) glycylglycine (Gly-Gly) in D_2O at pD 6.5, (B′) glycylglycine-$^{13}C_1$ (Gly-Gly-$^{13}COO^-$) in D_2O at pD 7.2, (C′) glycylglycine (Gly-Gly) in D_2O at pD 1.5, (D′) glycyl-β-alanine (Gly-β-Ala) in D_2O at pD 6.5, and (E′) L-alanyl-D-L-alanine in H_2O at pH 7 (solid line) and at pH 1.8 (dotted line). It should be noted that the carboxylate symmetric stretch in deuterated Gly-Gly does not decrease in intensity relative to the protonated species (Table 2), rather the intensity of the amide II′ band is much greater than that of the amide II and III bands. Spectra A, B, C, and D and A′, B′, C′, and D′ are obtained with 206.5-nm excitation, and spectra E and E′ are obtained with 218-nm excitation. Experimental conditions are the same as those in Figure 3. The sample concentrations were prepared at ca. 5 mM for 206.5-nm excitation, and ca. 50 mM for 218-nm excitation.

The enhancement of COO^- symmetric stretching is also observed in the resonance Raman spectra of Gly-Gly and other dipeptides with excitation on the long wavelength side of the amide $\pi \rightarrow \pi^*$ transition. Figure 5 shows the 206.5 nm excited resonance Raman spectra of Gly-Gly and its derivatives in H_2O and in D_2O, respectively. The resonance enhancement pattern of Gly-Gly (Figure 5a) is essentially identical to that of Ace-Gly. The strongly enhanced amide II and amide III bands of Gly-Gly occur at 1286 and 1576 cm^{-1}, respectively, while the amide II′ band of *N*-D-Gly-Gly occurs at 1496 cm^{-1} (Figure 5a′). The amide II′ band is mainly CN stretching; replacement of the NH by ND decouples CN and NH bending motions.[19] The Raman cross sections of the enhanced bands of Gly-Gly increase approximately 2-fold compared to those of Ace-Gly (Table 2) due to the 40% increased absorbance of Gly-Gly at 206.5 nm.

The 1403-cm^{-1} band of Gly-Gly in H_2O derives from the overlap of the $C_\alpha H_2$ symmetric bending vibration and the enhanced symmetric COO^- stretching vibration. We have previously reported that the ca. 1400-cm^{-1} band of Gly-Gly at pH 7 down shifts by ca. 15 cm^{-1} upon $C^{18}OO^-$ substitution.[30]

We can easily remove the contribution of symmetric COO^- stretch by protonation or esterification of the carboxylate group; the intensities of the 1396-cm^{-1} bands of Gly-Gly-Me and Gly-Gly at pH 1 (Figures 5b and 5c) decrease by ca. 2-fold. The remaining intensity at 1396 cm^{-1} results from the CH_2 symmetric bending vibration, which disappears when the hydrogens of the C_α carbon are replaced by methyl groups (Figure 5e, dotted line) or deuteriums. (Figure 5e′, dotted line). The enhancement of the $C_\alpha H_2$ bending vibration of Gly-Gly probably derives from the same source as the enhancement of the $C_\alpha H_3$ sb of NMA; the contribution of CC stretching to the normal mode causes enhancement due to the contraction of the C−C bond in the amide $\pi\pi^*$ excited state compared to the ground state.[19] The $C_\alpha H_2$ bending mode is not enhanced in *N*-D Gly-Gly, just as the $C_\alpha H_3$ sb mode is not enhanced in CH_3-$CONDCH_3$.[19]

The 1395 cm^{-1} band of *N*-D-Gly-Gly down shifts 16 cm^{-1} to 1379 cm^{-1} upon $^{13}COO^-$ substitution (Figure 5b′). This is comparable to the 14 cm^{-1} downshift of the 1411-cm^{-1} COO^- symmetric stretch of Gly upon $^{13}COO^-$ substitution. The 1395-cm^{-1} putative COO^- symmetric stretching mode in *N*-D-Gly-Gly spectrum (Figure 5a′) disappears in the *N*-D-Gly-Gly-OMe spectrum (Figure 5c′).

This COO^- symmetric stretch in Ace-Gly, Gly-Gly, and other dipeptides shows a ca. 20-fold increased 206.5 nm Raman cross section, compared to that in Gly and compared to that of carboxylates separated from the amide group by two or more methylene spacers, such as in Ace-β-Ala and Gly-β-Ala, for example. This increased enhancement of both the COO^- symmetric stretch and the amide vibrations correlates with an increased absorbance at 197 nm in Ace-Gly and Gly-Gly (Figures 2c and 2d).

Although the COO^- symmetric stretching band is relatively strong with visible Raman excitation, it is relatively weak with UV excitation. The COO^- symmetric stretch Raman cross section is 0.4 and 0.5 mbarns/str for acetic acid and Gly with 218-nm excitation, respectively, and ca. 15 and ca. 20 mbarns/str for 206.5-nm excitation, respectively (Table 2). A preresonance *A* term fit[37] for the COO^- symmetric stretch of acetic acid[9c] and Gly (Figure 6) shows that the resonance enhancement derives from a far-UV electronic transition at ca. 172 nm (Table 3), presumably from the NV_1 carboxylate $\pi\pi^*$ transition.[7,9c]

The Ace-Gly doublet (1305/1325 cm^{-1}) observed at pH 7 probably derives from a NMA-amide-III-like vibration (1315 cm^{-1}) vibrationally mixed with the $C_\beta H_2$ ($CH_3CONHC_\beta H_2$-$COO-$) symmetric bending vibration, which occurs at ca. 1318 cm^{-1} in the Raman spectra of Gly-Gly (Figure 5a); this doublet band is sensitive to the methylene $^{13}C_\beta$ substitution (Figure 3d) in Ace-Gly. In fact, this doublet becomes a singlet 1315-cm^{-1} band at pH ca. 1 (Figure 3c, dotted line). This proposed mixing of the methylene motion with the amide III band in Ace-Gly, which results in multiple amide III type bands, is consistent with previous studies of Oboodi et al. on Ala-Ala.[38] In Gly-Gly in H_2O at pH 7, the 1318 cm^{-1} $C_\beta H_2$ symmetric bending band occurs as a shoulder of amide III band, but is absent in Gly-Gly in H_2O at pH 1 and in Gly-β-Ala at pH 7. This $C_\beta H_2$ symmetric bending in dipeptides apparently gains some resonance enhancement, in contrast to the lack of resonance enhancement for the $C_\beta H_3$ sb mode in NMA.[10a,19,39]

The carboxylic acid carbonyl stretch found at 1749 cm^{-1} in Gly-Gly at pH 1.7 (Figure 5b) and the ester carbonyl stretch at

(38) (a) Oboodi, M. R.; Alva, C.; Diem, M. *J. Phys. Chem.* **1984**, *88*, 501. (b) Diem, M.; Lee, O.; Robert, G. M. *J. Phys. Chem.* **1992**, *96*, 548. (c) Robert, G. M.; Lee, O.; Diem, M. *J. Am. Chem. Soc.* **1988**, *110*, 1749.

(39) Wang, Y.; Purrello, R.; Georgiou, S.; Spiro, T. G. *J. Am. Chem. Soc.* **1991**, *113*, 6368.

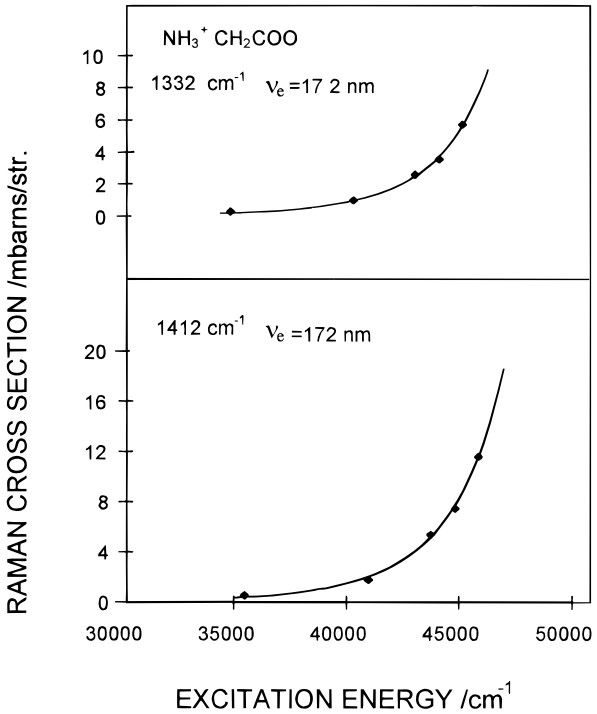

Figure 6. Raman excitation profiles of the glycine carboxylate symmetric stretch (1412 cm^{-1}) and the CH_2 bending vibration (1332 cm^{-1}) at pH 6.5. The solid lines correspond to nonlinear least-squares best fits of preresonance data to the Albrecht *A*-term expression (see Table 2).[37]

Table 3. Depolarization Ratios of Glycylglycine (Gly-Gly), Glycyl-*β*-alanine (Gly-*β*-Ala) , Glycine (Gly) and *N*-Methylacetamide (NMA)

vibrations (cm^{-1})	compds	ρ (488 nm)	ρ (244 nm)	ρ (206.5 nm)
amide III band				
1315	NMA	0.33	0.33	0.33
1286	Gly-Gly pH 7	0.20	0.26	0.28
1288	Gly-Gly pH 1	0.24	0.32	0.34
1283	Gly-*β*-Ala	0.25	0.33	0.33
amide II band				
1580	NMA	0.22	0.34	0.34
1576	Gly-Gly pH 7	0.25	0.28	0.27
1578	Gly-Gly pH 1	0.23	0.32	0.33
1579	Gly-*β*-Ala	0.23	0.33	0.32
symmetric COO^- stretch				
1440	acetic acid	0.09	0.18	0.27
1411	Gly pH 7	0.21	0.29	0.29
1396	*N*-D-Gly-Gly pH 7	0.55	0.51	0.43
1396	Gly-Gly pH 7	0.53	0.50	0.41
1395	TMA-Gly	0.57	0.51	0.43

1750 cm^{-1} in Gly-Gly-OMe (Figure 5c) are weakly enhanced with 206.5-nm excitation. The 206.5 nm Raman cross section of the carboxylic acid carbonyl stretch is 4-fold greater than that in glycine at pH 1. This suggests the existence of some interaction between the amide excited state and that of the protonated carboxylate groups. However, the Raman cross section of the carboxylic acid carbonyl stretch is 15-fold smaller than that of the COO^- symmetric stretch, indicating this interaction is much weaker than that between the amide and carboxylate groups.

Raman Excitation Profile and Depolarization Ratio Measurements. Resonance Raman spectra of Gly-*β*-Ala in H_2O and D_2O (Figures 5d and 5d′) show that addition of a methylene spacer between the amide and the carboxylate groups causes the resonance enhancement of the carboxylate stretching vibration to disappear. In addition, this additional methylene spacer

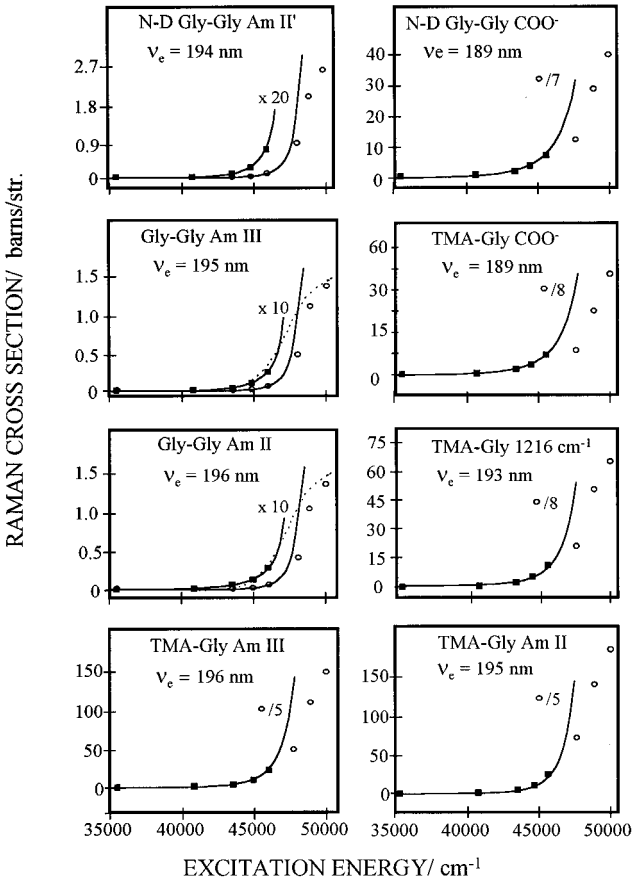

Figure 7. Raman excitation profiles of the carboxylate symmetric stretching, the amide II, III, and II′ bands, and the 1216-cm^{-1} band of TMA-Gly. The solid lines correspond to nonlinear least-squares best fits of preresonance data to the Albrecht *A*-term expression[37] to excitation wavelength between 210 and 300 nm. The dashed lines are the Gly-Gly absorption spectra at pH 7. The 228.5 and 244 nm Raman cross sections derive from CW laser excited Raman spectra with powers of 4 and 8 mW and accumulation times of ca. 5 min, respectively. The 217, 225, and 283 nm Raman cross sections were measured by using 6 ns pulsed laser excitation at a 20 Hz repetition rate with pulse energies of ca. 0.25, 0.25, and 0.5 mJ, with an accumulation time of ca. 6 min, respectively. Sample concentrations: ca. 0.25 M for 283-nm excitation, ca. 0.12 M for 244-nm excitation, ca. 80 mM for 225-nm excitation, and ca. 40 mM for 217-nm excitation.

decreases the amide II and III band Raman cross sections by 35% (Table 2). The increased cross sections of both the carboxylate symmetric stretch and the amide vibrations when the carboxylate is adjacent to the amide group, such as in Gly-Gly, Ace-Gly, and other dipeptides, suggest the presence of an electronic transition, which can enhance both the amide and carboxylate vibrations.

Evidence for this new transition comes from the Raman excitation profiles of the amide and carboxylate bands. Figures 6 and 7 show the excitation profiles of these bands in Gly, Gly-Gly, TMA-Gly, and *N*-D-Gly-Gly. The solid curves derive from Albrecht *A*-term fits[37] of excitation profile data, and these fits estimate the preresonant electronic transition frequencies for the enhanced vibrations. Table 2, which lists these resonance excited state transition frequencies, indicates that the symmetric carboxylate stretching (1414 cm^{-1}) and symmetric CH_2 bending vibrations (1332 cm^{-1}) of Gly are enhanced by an electronic transition at ca. 172 nm. In contrast, the symmetric COO^- stretching vibrations in Gly-Gly in D_2O and in TMA-Gly are enhanced by transitions at ca. 190 nm, and at 189 nm (Figure 7), respectively. Thus, the transition enhancing the symmetric

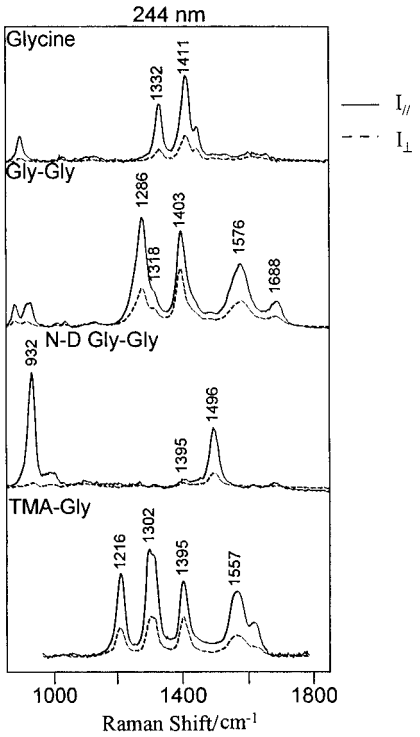

Figure 8. Representative 244 nm excited polarized (solid line) and depolarized (dashed line) Raman spectra used for depolarization ratio measurements. The 244-nm excitation utilized the ca. 10 mW CW laser, and the spectra were accumulated over a period of ca. 3 min. The sample concentrations were prepared near 150 mM. The spectral resolution is ca. 5 cm^{-1}.

carboxylate stretching red shifts by ca. 5500 cm^{-1} in dipeptides compared to that in Gly.

The amide I, II and III vibrations of NMA are enhanced by a transition at ca. 185 nm,[19,40] while the amide II and III bands of TMA-Gly are enhanced by a transition which is further red shifted to ca. 195 nm. In Gly-Gly the amide II and III resonance transitions occur between 194 and 196 nm. Similarly, the amide II' resonance transition of Gly-Gly in D_2O occurs at 194 nm. For all of these dipeptides, the resonant transition frequency for the COO^- symmetric stretching vibration occurs ca. 1300 cm^{-1} higher in energy than that of the amide vibrations.

Figure 8 displays examples of the measured 244 nm polarized and depolarized Raman spectra, while Table 3 lists the depolarization ratios of the amide II and III bands, and of the symmetric COO^- stretching band with 206.5-, 244-, and 488-nm excitations. If the Raman cross section were dominated by a single non-degenerate electronic transition, a single component of the Raman tensor would dominate, and $\rho = 0.33$. This is exactly the depolarization ratio observed for the amide III band of aqueous NMA for excitation wavelengths between 488 and 206.5 nm. In the case of Gly-β-Ala and Gly-Gly at pH 1, where little interaction occurs between the carboxylate and amide groups, ρ approaches 0.33 as excitation occurs close to resonance with the amide $\pi \rightarrow \pi^*$ transition. The $\rho = 0.33$ value for $\lambda \leq 244$ nm indicates that the enhancement of the amide III mode, in both Gly-β-Ala at pH 7 and Gly-Gly at pH 1, is dominated by the single amide $\pi \rightarrow \pi^*$ transition, in a manner similar to that in NMA. In contrast, ρ for the amide III band of Gly-Gly at pH 7 is smaller than 0.33 for all measured excitation wavelengths, which suggests that this resonance Raman enhancement derives from at least two electronic transitions.[19b,41a]

(40) Dudik, J. M.; Johnson, C. R.; Asher, S. A. *J. Phys. Chem.* **1985**, *89,* 3805.

The ρ value of the symmetric COO^- stretch of Gly and FC is much smaller than 0.33 for visible excitation, but begins to approach this value as excitation approaches preresonance with the 174 nm carboxylate $\pi \rightarrow \pi^*$ transition. The ρ value of the symmetric COO^- stretching vibration in Gly-Gly and other dipeptides exceeds 0.40 for excitation even in resonance, a behavior dramatically different from that in Gly and FC (Table 3). The symmetric COO^- stretch of Gly-Gly should be quite similar to that in Gly. A ρ value higher than 0.40 indicates that the resonance Raman enhancement of the symmetric COO^- stretching of Gly-Gly must derive from a Raman scattering tensor with at least two diagonal elements; this requires enhancement by at least two different preresonant electronic transitions.[41]

Discussion

Dipeptides are known to have a strong amide $\pi \rightarrow \pi^*$ transition at ca. 185 nm and a weaker carboxylate $\pi \rightarrow \pi^*$ transition at ca. 170 nm. Our results indicate that an additional electronic transition occurs at ca. 200 nm for dipeptides at neutral pH. The evidence for this transition is the following: (1) the occurrence of an absorbance increase in aqueous dipeptides around 200 nm which give rise to a band at 197 nm ($\epsilon \approx 3000$ M^{-1} cm^{-1}) in the absorption difference spectrum between the dipeptide absorption spectrum and the sum of the spectra of FC and NMA; (2) the 206.5 nm Raman cross sections increase 4-fold for the amide vibrations and 20-fold for the carboxylate vibrations in dipeptides at pH 7, compared to the amide vibrations in NMA and for the carboxylate vibration in simple acids such as formic acid; (3) the resonance enhancement transition frequency, ν_e, is ca. 1300 cm^{-1} higher for the carboxylate symmetric stretch than for the amide vibrations (which we know are selectively enhanced by the amide $\pi \rightarrow \pi^*$ transition); (4) the Raman depolarization ratios of amide and carboxylate vibrations indicate the involvement of at least two electronic transitions; and (5) the absorption and Raman spectra of aqueous dipeptides dramatically change upon carboxylate protonation. The spectra then mimic NMA.

This new transition cannot be assigned to the $n \rightarrow \pi^*$ transition of amides and carboxylates, because the $n \rightarrow \pi^*$ transition oscillator strengths are known to be weak, and their resonance Raman enhancements should be negligible.[40] The amide and carboxylate higher energy NV_2 $\pi \rightarrow \pi^*$ transitions are at too high energies to contribute to absorption at ca. 200 nm.

This new transition results from the interactions between the amide and carboxylate groups through a mechanism which involves either exciton interaction between the transitions or interactions between the excited electronic states. Either mechanism is likely to lead to the same result.[22,42] Figure 9a shows a simplified molecular orbital picture of the frontier orbitals of the amide and carboxylate groups. The ground state amide and carboxylate n and π orbitals differ significantly in energy. We assume that the n and π orbitals do not interact and remain localized on the amide and carboxylate groups. The excited state π^* orbitals of the amide and carboxylate groups interact to form molecular orbitals A and B, which are linear combinations of the amide π^* and carboxylate π^* orbitals. Because the energies of the amide and carboxylate π^* orbitals significantly differ, the A orbital will be dominated by the amide π^* orbital, while the B orbital will be dominated by the carboxylate π^* orbital.

(41) (a) Long, D. A. *Raman Spectroscopy*; McGraw-Hill: New York, 1977. (b) Udagawa, Y.; Iijima, M.; Ito, M. *J. Raman Spectrosc.* **1974**, *2*, 315.

(42) Cantor, C. R.; Schimmel, P. R. *Biophysical Chemistry, II,* W. H. Freeman and Company, San Francisco, 1980; p 367.

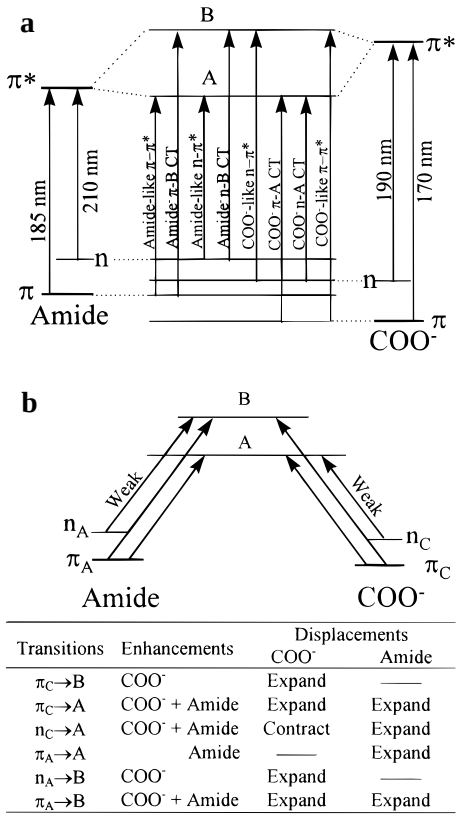

Transitions	Enhancements	Displacements COO⁻	Displacements Amide
$\pi_C \rightarrow B$	COO^-	Expand	——
$\pi_C \rightarrow A$	COO^- + Amide	Expand	Expand
$n_C \rightarrow A$	COO^- + Amide	Contract	Expand
$\pi_A \rightarrow A$	Amide	——	Expand
$n_A \rightarrow B$	COO^-	Expand	——
$\pi_A \rightarrow B$	COO^- + Amide	Expand	Expand

Figure 9. (a) Schematic energy level diagram of the frontier orbitals of isolated amide and carboxylate groups, proposed orbital mixing, and possible resulting electronic transitions. The measured absorption spectra indicate the relative ordering of the filled n and π orbitals, and the unfilled π^* orbitals of the carboxylate and amide groups. The measured transition energy of the charge transfer band locates the relative energy difference between the n orbitals of the amide and carboxylate. We are less certain of the relative ordering of the filled π orbitals. (b) Possible charge transfer transitions, vibrational enhancements, and excited state displacements.

The COO^- $\pi_C \rightarrow$B transition is similar to that of the carboxylate $\pi \rightarrow \pi^*$ transition and is localized mainly in the carboxylate group. However, this transition occurs at a frequency slightly higher than that of the carboxylate. Similarly, the amide $\pi_A \rightarrow$A transition resembles the amide $\pi \rightarrow \pi^*$ transition, but will be slightly red shifted. The amide $n_A \rightarrow$A transition should be similar to the amide $n \rightarrow \pi^*$ transition and have a very weak oscillator strength, as should the $n_C \rightarrow$B transition. The new transition could derive from charge transfer (CT) transitions from either the COO^- n_C or π_C orbitals to the amide A orbital, or from the amide n_A or π_A orbitals to the B orbital (Figure 9b).

The amide vibrations will be enhanced mainly by the $\pi_A \rightarrow$A, $\pi_A \rightarrow$B, $\pi_C \rightarrow$A, or $n_C \rightarrow$A transition. In each case, the bond order decreases either due to removal of electron density from a bonding amide orbital or because electron density is transferred into an antibonding amide orbital. These bond order changes result in Raman enhancement due to the resulting excited state geometry alterations (bond elongations), which result in significant Raman Franck−Condon factors (*vide infra*). An additional source of enhancement can occur due to bond force constant changes. The $n_A \rightarrow$B transition is unlikely to lead to much enhancement of the amide vibrations, since little change should occur in the amide bond order.

The carboxylate vibration will be enhanced by the $\pi_C \rightarrow$B, $\pi_C \rightarrow$A, and $\pi_A \rightarrow$B transitions. Each transition decreases the carboxylate bond order and results in an excited state expansion. The $n_C \rightarrow$A transition will also enhance the carboxylate vibration, even though no direct bond order change occurs through the transfer of the nonbonding electron from the carboxylate to the amide group; however, the $n_C \rightarrow$A electronic transition changes the anionic carboxylate group to a neutral radical. The decreased electron repulsion causes the carboxylate group bonds to contract.[43]

The resonance Raman excitation profile and the Raman depolarization ratio measurements can help assign these transitions. The magnitude and dispersion of the Raman cross sections give information on the resonance enhancing excited state transition frequency. The depolarization ratios give information on the number of enhancing transitions.

The resonance Raman cross section is proportional to the square of the sum of the Raman scattering tensor elements, which have contributions from all of the electronic excited states.[44] For the case of resonance enhancement by only two electronic transitions, the resonance Raman cross section, σ, of a symmetric vibration can be expressed in the Kramers−Heisenberg−Dirac (KHD) formalism,

$$\sigma \approx |\hat{\alpha}|^2 = |\hat{\alpha}_1 + \hat{\alpha}_2|^2 = \left| \sum_{\sigma} \sum_{\rho} \hat{M}^1_{\rho} \hat{M}^1_{\sigma} \sum_{\nu_1} \frac{\langle 1|\nu_1\rangle\langle\nu_1|0\rangle}{\Delta\nu_{\nu_1} - i\Gamma_1} + \hat{M}^2_{\rho} \hat{M}^2_{\sigma} \sum_{\nu_2} \frac{\langle 1|\nu_2\rangle\langle\nu_2|0\rangle}{\Delta\nu_{\nu_2} - i\Gamma_2} \right|^2 \quad (4)$$

where $\hat{\alpha}$ is the total Raman tensor and $\hat{\alpha}_1$ and $\hat{\alpha}_2$ are the individual Raman tensors associated with enhancement by electronic transitions to excited state states, 1 and 2, respectively. $\hat{M}^1_{\rho}$ and $\hat{M}^2_{\rho}$, and $\hat{M}^1_{\sigma}$ and $\hat{M}^2_{\sigma}$ are the electronic transition moments along particular Cartesian coordinates, ρ and σ, of electronic excited state 1 or 2, respectively. ν_1 and ν_2, and Γ_1 and Γ_2 are the excited state vibrational levels of the mode of interest, and the homogeneous line widths of states 1 and 2, respectively. ΔV_{ν_2} and ΔV_{ν_1} are the frequency offsets between the laser frequency and the transition frequencies to the vibronic levels ν_1 and ν_2 of electronic excited states 1 and 2.

The depolarization ratio, ρ, for a non-degenerate symmetric vibration for the case of only two diagonal tensor elements, is given by,[45]

$$\rho = \frac{1 + 3\delta^2}{8 + 4\delta^2} \quad (5)$$

where, $\delta = |\alpha_{xx} - \alpha_{yy}|/|\alpha_{xx} + \alpha_{yy}|$, and α_{xx} and α_{yy} are the tensor elements of the Raman polarizability, α, in the diagonal frame of the Raman polarizability tensor. The orientation of the frame depends on the relative contribution to the Raman polarizability of the electronic transitions to excited states 1 and 2. The Appendix derives quantitative relationships between the relative orientation of these electronic transitions and their resonance Raman enhancements, and the relative magnitudes of the two diagonal Raman tensor elements. Equations 6 and 7 relate the relative values of the Raman tensor elements in the diagonal frame to the relative magnitudes of the Raman

(43) The C−O bond lengths of the protonated carboxyl group of acetylglycine are 1.196 and 1.306 Å (Donohue, J.; Marsh, R. E. *Acta Crystallogr.* **1962**, *15*, 941). The C−O bond lengths of the deprotonated carboxylate group of alanylglycine are 1.263 and 1.260 Å (Koch, M. H. J.; Germain, G. *Acta Crystallogr. Sect. B* **1970**, *26*, 410). The average C−O bond length in the protonated carboxyl group contracts by 0.011 Å compared to that of the deprotonated carboxylate group.

(44) Myers, A. B.; Mathies, R. A. *Biological Applications of Raman Spectroscopy*; Spiro, T. G., Ed.; John Wiley & Sons Inc.: New York, 1987; Vol. 2, p 1.

(45) Li, P.; Sage, J. T.; Champion, P. M. *J. Chem. Phys.* **1992**, *97*, 3214.

polarizability contributed by the individual electronic transitions oriented at angle φ between them:

$$\alpha_{xx} + \alpha_{yy} = \alpha_1 + \alpha_2 \quad (6)$$

and

$$\alpha_{xx}\alpha_{yy} = \alpha_1\alpha_2 \sin^2 \varphi \quad (7)$$

Equation 7 shows that the relative sign of the diagonal Raman tensor elements, α_{xx} and α_{yy}, is independent of angle φ, and that the relative sign of α_{xx} and α_{yy} in the diagonal frame is identical to that of the individual Raman tensor elements, α_1 and α_2.

For the case of the amide vibrations, a value of $\rho < 0.33$ indicates that $\delta < 1$ in eq 5, and that α_{xx} and α_{yy}, and consequently α_1 and α_2, are of the same sign. This means that the Raman enhancement by the putative CT transition and the amide-like $\pi\rightarrow\pi^*$ transitions must result in constructive interference[46] for the amide vibrations. This constructive interference between the CT and the amide $\pi\rightarrow\pi^*$ transitions would increase the Raman cross section dispersion for the amide vibrations, and red shift the ν_e calculated from the Albrecht *A*-term expression.

In contrast, for the carboxylate symmetric stretching vibration, the measured value of $\rho > 0.33$ indicates that $\delta > 1$, and requires opposite signs for the diagonal tensor elements, α_{xx} and α_{yy}, and consequently for α_1 and α_2 (eq 7). This means that for the carboxylate symmetric stretching vibration, the CT and the carboxylate-like $\pi\rightarrow\pi^*$ transitions will show destructive interference. This destructive interference would decrease the preresonance excitation profile curvature at the low-energy side of the CT band, and would lead to an increased calculated preresonant *A*-term transition frequency, ν_e. These predictions are exactly what we observe for the preresonance Raman dispersion of the amide and carboxylate vibrations, where ν_e is 1300 cm^{-1} higher for carboxylate symmetric stretch than for the amide vibrations (Figure 7).

The sign of a Raman tensor contribution for a single electronic transition, α_i, is determined by the energy denominator and by the sign of the Raman Franck−Condon factor[44] (eq 4, where we assume *M* is a real quantity). Since our excitation is in the preresonance region ($\Delta\nu_v > 0$), the sign of α only depends upon the Franck−Condon factors. These Raman Franck−Condon factors are dominated by the $<1|1><1|0>$ and $<1|0><0|0>$ vibronic transitions, since in the typically small excited state displacement limit, $<2|0>$ is very small. The $<1|0>$ or $<0|1>$ Franck−Condon factors scale with Δ, the displacement of the excited state along the normal coordinate of the vibration of interest. If two transitions dominate the preresonance Raman enhancement, and if their contributions are of opposite sign, then the displacements of the excited state geometry in the two transitions will be of opposite sign along the vibrational coordinate; i.e. one transition gives rise to an expansion, and the other gives rise to a contraction.

We can use this information to assign the new CT electronic transition at ca. 200 nm in Gly-Gly at pH 7. We previously established that the amide C−N and C═O bonds expand during the amide $\pi\rightarrow\pi^*$ transition.[19] The fact that $\rho < 0.33$ for the amide II and III bands of Gly-Gly (pH 7) indicates that the displacements, Δ, resulting from the CT and amide $\pi\rightarrow\pi^*$ transitions have the same sign. This requires that the CT transition expand the amide C−N and C═O bonds, as does the amide $\pi\rightarrow\pi^*$ transition. In contrast, the $\rho > 0.33$ value for the carboxylate vibration of Gly-Gly at pH 7 requires that the CT transition contracts the carboxylate group, in contrast to the expansion caused by the carboxylate $\pi\rightarrow\pi^*$ transition; the carboxylate $\pi\rightarrow\pi^*$ transition expands the carboxylate C−O bonds since the bond orders decrease upon electron transfer from a bonding to an antibonding orbital.

Figure 9b shows that the $n_C\rightarrow$A CT transition simultaneously expands the amide group and contracts the carboxylate group. This CT transition populates the antibonding amide localized A orbital and decreases the amide C−N and C═O bond orders, causing them to expand. In addition, this $n_C\rightarrow$A CT transition decreases the electron density in the carboxylate nonbonding orbital; the decreased electron repulsion of the neutral carboxylate compared to the anion results in a contraction of the carboxylate C−O bonds.[43] An alternative argument, which compares the analogous allene allyl and radical, also predicts that the carboxylate radical bond lengths would decrease compared to the anion.[47]

The carboxylate vibration is enhanced by the CT transition and by the $\pi_C\rightarrow$B transition, which have carboxylate displacements of opposite sign. Thus, α_{xx} and α_{yy} for the carboxylate symmetric stretch will be of opposite sign, and $\rho > 0.33$. The amide vibrations, in contrast, will have α_{xx} and α_{yy} values of identical sign and show a $\rho < 0.33$ value for the amide vibrations.

Exactly the opposite behavior would occur if the charge transfer transition were from the carboxylate π orbital to A orbital. This is because the carboxylate $\pi\rightarrow$A transition would reduce the carboxylate π bond order, which would result in an expansion of the carboxylate C═O bonds. The carboxylate expansion due to the $\pi\rightarrow$A charge transfer transition and carboxylate-like $\pi\rightarrow\pi^*$ transition would result in identical signs for the Raman tensor elements and give $\rho < 0.33$.

We can also exclude CT transitions from the amide n and π orbitals to the B orbital, because they would also result in expansions of the carboxylate group. In addition, these transitions should occur at much higher frequencies. This carboxylate $n_C\rightarrow$A CT transition simultaneously changes the electronic density at the amide and carboxylate groups and alters their geometries, and should result in resonance Raman enhancements of both the amide and carboxylate vibrations. A similar charge transfer transition appears not to occur in Gly-β-Ala, because of the decreased spatial overlap between the carboxylate and amide π^* orbitals (Figure 9a). This transition does not occur in Gly-Gly at pH 1, presumably because the deprotonated carboxylate π^* orbital is at a much higher energy, which dramatically decreases the mixing between the amide and the protonated carboxylate π^* orbitals. However, the weaker observed enhancement of the carbonyl C═O stretch in the carboxylic acid and ester form may indicate some coupling with a much smaller magnitude.

This CT transition that occurs across the bridging methylene group might be expected to enhance vibrations of the bridging methylene. In fact, we see enhancement of the 1318 cm^{-1} $C_\beta H$ symmetric bending vibration only for dipeptides such as Gly-Gly at pH 7, but see no enhancement of the same vibration in Gly-β-Ala, Gly-Gly-Me, or Gly-Gly at pH 1.

We conclude that the interactions between the amide and the carboxylate groups of dipeptides result in a new charge transfer electronic transition at ca. 197 nm with a molar absorptivity of ca. 3000 cm^{-1} M^{-1}. Our Raman excitation profile and depolarization ratio results allow us to assign this band to a charge transfer transition of an electron from a mainly carboxylate n orbital to a mainly amide π^* orbital.

(46) (a)Shin, K-S. K.; Zink, J. I. *J. Am. Chem. Soc.* **1990**, *112*, 7148. (b) Hildebrandt, P.; Tsuboi, M.; Spiro, T. G. *J. Phys. Chem.* **1990**, 94, 2274.

(47) Salem, L. *The Molecular Orbital Theory of Conjugated Systems*; W. A. Benjamin, Inc.: Reading, MA, 1966; p 65.

The existence of this charge transfer transition in the deep UV explains the previously observed facile photochemical decarboxylation of dipeptides.[8] This CT absorption would be involved in photoinduced electron transfer, where the carboxylate group acts as an electron donor and the amide group acts as an electron acceptor. The resulting carboxylate radical appears to be dissociatively unstable; scission occurs with the loss of a carbon dioxide. This charge transfer is likely to occur at the penultimate carboxylate end of all peptides and proteins.

A similar coupling of the adjacent amide transitions may occur in peptides and proteins, and in principle, could give rise to an extended charge transfer conduit for electron transfer through delocalized excited states of the peptide backbone.[25] The extent of the delocalization could depend on the protein secondary structure. We are in the process of exploring these possibilities.

Conclusion

We have examined the UV resonance Raman and the VUV absorption spectra of aqueous glycylglycine and other dipeptides. We observed strong resonance Raman enhancement of the 1400 cm^{-1} symmetric COO^- stretch vibration. The 206.5 nm excited Raman cross section of the symmetric COO^- stretch increases 20-fold compared to that in acetate. An additional methylene spacer group situated between the amide and carboxylate groups causes the resonance Raman enhancement of the symmetric COO^- stretch to dramatically decrease. We also examined the excitation profiles, and the Raman depolarization ratio dispersion of glycylglycine, and the related analogs in order to elucidate the mechanism of the symmetric COO^- stretch enhancement. We use these data to detect and assign a new charge transfer transition in dipeptides, which involves electron transfer mainly from a nonbonding carboxylate orbital to a π^* orbital of the amide group. This transition should also be present at the penultimate carboxylate end of peptides and proteins. This transion may be important in peptide photochemistry and may serve as a conduit for electron transfer.

Acknowledgment. We gratefully acknowledge support from NIH grant R01GM30741−13 to S.A.A. We would also like to acknowledge Dr. John Clark Sutherland for use of the instrumentation at the National Synchrotron Light Source at Brookhaven National Laboratory for the VUV absorption spectral measurements. We acknowledge support from the Office of Health and Environmental Research, USDOE and the Office of Chemical Research and the Office of Materials Research, U. S. Department of Energy. We kindly thank Professor Peter Wipf for help in the peptide synthesis, Dr. Steve Geib for help in searching the dipeptide crystal data bank, and Professor Max Diem for providing the D-Ala-Ala sample. We also thank Professors R. Coalson, S. Mukamel, A. C. Albrecht, K. Jordan, and J. Grabowski for helpful discussions.

Appendix

Here we relate to the resonance Raman tensors associated with the individual electronic transitions to the molecular resonance Raman tensor in the diagonal frame. We assume that enhancement occurs by an Albrecht *A*-term mechanism, and is determined by the magnitude of the electronic transition moments and the Raman Franck−Condon factors of two separate transitions (Kramers−Heisenberg−Dirac (KHD) formalism).[41] We assume that we are very close to resonance, but in the preresonance regime where we can neglect the imaginary part of the Raman tensor elements.

We consider only two electronic dipole transitions, $\mathbf{M_1}$ and $\mathbf{M_2}$, oriented at an angle φ to each other. These two electronic transitions may occur in different regions of the molecule, but they enhance the same vibrational normal mode. We define two coordinate systems, Frame 1, $\{x_1, y_1, z_1\}$, and Frame 2, $\{x_2, y_2, z_2\}$, such that the $\mathbf{M_1}$ transition moment occurs along x_1 and the $\mathbf{M_2}$ transition occurs along x_2 and z_2 is parallel to z_1. These individual Raman tensors can be written:

$$\{\boldsymbol{\alpha_1}\} = \begin{bmatrix} \alpha_1 & 0 & 0 \\ 0 & 0 & 0 \\ 0 & 0 & 0 \end{bmatrix} \qquad \{\boldsymbol{\alpha_2}\} = \begin{bmatrix} \alpha_2 & 0 & 0 \\ 0 & 0 & 0 \\ 0 & 0 & 0 \end{bmatrix} \quad \text{(A-1)}$$

The total Raman tensor, $\boldsymbol{\alpha}$, in the coordinate Frame 1 can be expressed

$$\boldsymbol{\alpha} = \begin{bmatrix} \alpha_1 & 0 & 0 \\ 0 & 0 & 0 \\ 0 & 0 & 0 \end{bmatrix} + R^{\mathrm{T}} \begin{bmatrix} \alpha_2 & 0 & 0 \\ 0 & 0 & 0 \\ 0 & 0 & 0 \end{bmatrix} R \quad \text{(A-2)}$$

where R is the transformation matrix that rotates coordinate Frame 2 into Frame 1:

$$R = \begin{bmatrix} \cos\varphi & \sin\varphi & 0 \\ -\sin\varphi & \cos\varphi & 0 \\ 0 & 0 & 1 \end{bmatrix} \quad \text{(A-3)}$$

Equation A.2 becomes:

$$\alpha = \begin{bmatrix} \alpha_1 + \alpha_2 \cos^2\varphi & \alpha_2 \cos\varphi \sin\varphi & 0 \\ \alpha_2 \cos\varphi \sin\varphi & \alpha_2 \sin^2\varphi & 0 \\ 0 & 0 & 0 \end{bmatrix} \quad \text{(A-4)}$$

This symmetric tensor can be diagonalized by rotating it about z_1 axis by angle θ,

$$\alpha^{\mathrm{d}} = \begin{bmatrix} \alpha_{xx} & 0 & 0 \\ 0 & \alpha_{yy} & 0 \\ 0 & 0 & 0 \end{bmatrix} \quad \text{(A-5)}$$

A tedious calculation gives,

$$\alpha_{xx} = \alpha_1 \cos^2\theta + \alpha_2 \cos^2(\varphi + \theta) \quad \text{(A-6)}$$

$$\alpha_{yy} = \alpha_1 \sin^2\theta + \alpha_2 \sin^2(\varphi + \theta) \quad \text{(A-7)}$$

$$\theta = {}^1/_2 \tan^{-1}[-\alpha_2 \sin(2\varphi)/(\alpha_1 + \alpha_2 \cos(2\varphi))] \quad \text{(A-8)}$$

From which we obtain:

$$\alpha_{xx} + \alpha_{yy} = \alpha_1 + \alpha_2 \quad \text{(A-9)}$$

$$\alpha_{xx}\alpha_{yy} = \alpha_1\alpha_2 \sin^2\varphi \quad \text{(A-10)}$$

Equation A.9 is expected, since the trace of a symmetric tensor is invariant. Equation A.10 displays an important result, which we believe has not previously been recognized. This expression relates the angle φ between the transition dipoles to the relative value of the two Raman tensor elements in the diagonal frame. This equation is valid when only two enhancing resonance transitions occur, and indicates that, given a relative value of α_1 and α_2, which are the separate Raman polarizability tensor elements for each transition, we can use the measured relative values of α_{xx} and α_{yy} determined by an isotropic solution depolarization ratio measurement to calculate the angle φ between the transition moment dipoles.[16] This expression is specified for any excitation wavelength. Of course, the relative values of α_{xx} and α_{yy} vary with excitation wavelength.

JA960421+